Dissociative Excitation Energy Transfer in the Reactions of Protonated Cysteine and Tryptophan with Electronically Excited Singlet Molecular Oxygen (a$^1\Delta_g$)

Fangwei Liu, Yigang Fang, Yun Chen, and Jianbo Liu*

Department of Chemistry and Biochemistry, Queens College and the Graduate Center of the City University of New York, 65-30 Kissena Boulevard, Flushing, New York 11367, United States

ABSTRACT: We report a study on the reactions of protonated cysteine (CysH$^+$) and tryptophan (TrpH$^+$) with the lowest electronically excited state of molecular oxygen (O$_2$, a$^1\Delta_g$), including the measurement of the effects of collision energy (E_{col}) on reaction cross sections over the center-of-mass E_{col} range of 0.05 to 1.0 eV. Electronic structure calculations were used to examine properties of complexes, transition states and products that might be important along the reaction coordinate. For CysH$^+$ + ^{1}O$_2$, the product channel corresponds to C$^\alpha$−C$^\beta$ bond rupture of a hydroperoxide intermediate CysOOH$^+$ accompanied by intramolecular H atom transfer, and subsequent dissociation to H$_2$NCHCO$_2$H$^+$, CH$_3$SH and ground triplet state O$_2$. The reaction is driven by the electronic excitation energy of ^{1}O$_2$, the so-called dissociative excitation energy transfer. Quasi-classical direct dynamics trajectory simulations were calculated for CysH$^+$ + ^{1}O$_2$ at E_{col} = 0.2 and 0.3 eV, using the B3LYP/6−21G method. Most trajectories formed intermediate complexes with significant lifetime, implying the importance of complex formation at the early stage of the reaction. Dissociative excitation energy transfer was also observed in the reaction of TrpH$^+$ with ^{1}O$_2$, leading to dissociation of a TrpOOH$^+$ intermediate. In contrast to CysOOH$^+$, TrpOOH$^+$ dissociates into a glycine molecule and *charged* indole side chain in addition to ground-state O$_2$ because this product charge state is energetically favorable. The reactions of CysH$^+$ + ^{1}O$_2$ and TrpH$^+$ + ^{1}O$_2$ present similar E_{col} dependence, i.e., strongly suppressed by collision energy and becoming negligible at E_{col} > 0.5 eV. This is consistent with a complex-mediated mechanism where a long-lived complex is critical for converting the electronic energy of ^{1}O$_2$ to the form of internal energy needed to drive complex dissociation.

I. INTRODUCTION

Despite its apparent simplicity, molecular oxygen possesses a unique electronic configuration with a singlet excited state (O$_2$[a$^1\Delta_g$], the lowest electronically excited state, commonly called singlet oxygen) lying above its triplet ground state (O$_2$[X$^3\Sigma_g^-$]).[1] ^{1}O$_2$ has a characteristic chemistry in which molecules are oxygenated,[2−7] setting it apart from ground-state O$_2$ which, because of two unpaired parallel-spin electrons, does not react with most molecules unless activated by additional energy. ^{1}O$_2$ can be generated in biological systems by energy transfer to ground-state O$_2$ from protein-bound or other chromophores on exposure to UV and visible light (*vide infra*), and by a range of enzymatic and nonenzymatic reactions including those mediated by heme proteins, lipoxygenases, activated leukocytes, and radical termination reactions.[8] Consequently, ^{1}O$_2$-mediated oxygenation reactions are involved in the progression of cell death, aging and diseases (e.g., cataract, sunburn, and some skin cancers),[8−10] and in photodynamic therapy where ^{1}O$_2$ is used to kill cancer cells.[11] Proteins are the major target for ^{1}O$_2$-mediated oxidative damage due to their high abundance in living bodies. Cysteine (Cys) and tryptophan (Trp) are two of five amino acids that are most susceptible to oxidative damage by ^{1}O$_2$ because these residues have electron-rich side chains and thus are favored

by electrophilic oxidizers.[8,10,12] In fact, because it is prone to oxidation, Cys is rarely present as a free residue at surface-exposed parts of a protein,[13] and oxidation of Cys by ^{1}O$_2$ often yield disulfide formation such as the dimeric product cystine.[14]

In addition to biological milieu, amino acids (including free amino acids as well as peptides and proteins) are ubiquitous in tropospheric particles and depositions, and undergo transformations due to photochemically formed reactive oxygen species including ^{1}O$_2$.[15−17] Cys and Trp are particularly easily decomposed in the atmosphere.[18,19] For instance, calculated half-lives for Cys and Trp range from seconds to minutes in typical wintertime, midday fog drops in Davis, the northern portion of California's Central Valley.[16] Consequently, Cys and Trp were found less commonly, or at lower concentration, in the atmospheric aerosols.[18]

Because of these biological and photochemical implications, there has been considerable interest in studying ^{1}O$_2$-mediated oxidation of Cys and Trp.[14,20−32] Most experiments were carried out in solution, and reaction products were identified using

chromatographic and spectrometric methods. In these experiments, ultraviolet or visible light in a specific wavelength region was used to create an excited state of a given molecule, a so-called photosensitizer, which in turn transferred its excitation energy to ground-state O_2 to generate $^1O_2$.[1] Giving the complexities of photosensitized oxidation reactions (e.g., pH, oxygen concentration, solvent composition, combination of light and sensitizers, competition between radical- and $^1O_2$-mediated reactions),[7] to unambiguously determine reaction mechanisms requires multiple sets of control experiments and can be a difficult endeavor. Consequently, several aspects of Cys and Trp oxidation including mechanisms, products and intermediates involved have yet to be fully characterized.[12] To circumvent the problems associated with solution-phase photooxidation experiments, our approach has been to study the reactions of protonated amino acids with chemically generated "clean" $^1O_2$ in the gas phase,[33,34] using electrospray-ionization (ESI)[35,36] and guided-ion-beam scattering methods.[37] To supplement our gas-phase experiment and help unravel the reaction mechanism, electronic structure calculations were used to find complexes, transition states and products along the reaction coordinate, and direct dynamics trajectory simulations were used to provide additional mechanistic insights. Compared to the study of $^1O_2$ reactions in solution, much less is known about the ion-chemistry with $^1O_2$ in the gas phase.[33,34,38−50] Note that most of recent ion−molecule reaction studies involving $^1O_2$ were reported by Viggiano and co-workers,[44−50] and were concentrating on the reactions of small negative ions with $^1O_2$ which are more relevant to ionospheric chemistry.

The remainder of the paper is organized as follows. Section II describes the guided-ion-beam scattering methods used to measure the gas-phase reactions of protonated cysteine (CysH$^+$) and tryptophan (TrpH$^+$) with $^1O_2$, and the electronic structure and quasi-classical trajectory methods used to investigate their reaction dynamics. Reaction results are presented in section III, starting with the products and cross sections of CysH$^+$ and TrpH$^+$ with $^1O_2$, and comparison with solution-phase photooxidation results, proceeding to the construction of the reaction coordinate for CysH$^+$ + $^1O_2$ and TrpH$^+$ + $^1O_2$ using density functional theory calculations, and finally to the analysis of dynamics trajectory results of CysH$^+$ + $^1O_2$. Conclusions are presented in section IV.

II. EXPERIMENTAL AND COMPUTATIONAL DETAILS

A. Experimental Procedures. The guided-ion-beam tandem mass spectrometer used in this study has been described in detail previously,[33,34,51,52] along with the operation, calibration and data analysis procedures. The apparatus consists of an ion source, radio frequency (rf) hexapole ion guide, quadrupole mass filter, rf octopole ion guide surrounded by a scattering cell, second quadrupole mass filter, and a pulse-counting detector. Both quadrupole mass filters use Extrel 9.5 mm trifilter rods, which were operated at 2.1 MHz to cover a mass/charge (m/z) range of 1−500. Sample solution was prepared in HPLC grade methanol/water (1:1 volume ratio) containing 0.5 mM L-cysteine hydrochloride (≥99.0%, Fluka), or a mixture of 0.5 mM L-Trp (99%, Acros) and hydrochloric acid (Riedel-de Haën). The solution was sprayed into the ambient atmosphere through an electrospray needle at a flow rate of 0.04 mL/h, and the electrospray needle was held at 3000 V relative to ground. Positively charged droplets

formed from electrospray were fed into a heated desolvation capillary assembly. The capillary was biased at 70 V relative to ground and heated to 170−180 °C. Charged liquid droplets and solvated ions underwent continuous desolvation as they passed through the heated capillary, converting to gas-phase ions and transported into the source chamber. A skimmer was located 2.5 mm from the end of the capillary, separating the source chamber and the hexapole ion guide. The skimmer was biased at 10 V relative to ground, and the electric field between the capillary and skimmer helped remove remaining solvent molecules attached to ions by collision-induced desolvation. Ions emerging from the skimmer were passed into a rf hexapole ion guide at a pressure of 20−30 mTorr, resulting in collisional focusing and thermalization of internal and translational energies of ions.[53−55] As characterized by a collision-induced dissociation experiment,[33] the internal energy of primary ions could be well described by a Maxwell−Boltzmann distribution at ∼310 K. Ions subsequently passed into the first quadrupole mass filter for mass selection. Mass-selected ions (CysH$^+$ or TrpH$^+$) were focused into an octopole ion guide that traps ions radially. The octopole passes through a scattering cell filled with neutral reactant gas. The cell pressure was measured by a capacitance manometer (MKS Baratron 690 head and 670 signal conditioner). The ion guide minimizes losses of the reactant and product ions resulting from scattering. After passing through the scattering cell, any product ions and the remaining protonated amino acids drifted to the end of the octopole where they were mass analyzed and counted using an electron multiplier.

The initial kinetic energy of the primary ion beam was determined using a retarding potential analysis (RPA),[56] i.e., the intensity of the primary ion beam was measured while sweeping the DC bias voltage applied to the octopole. The derivative of the onset energy was fit to a Gaussian distribution. The center of the fit defines the initial kinetic energy of the primary ion beam, and the full width at half-maximum (fwhm) of the distribution describes the kinetic energy spread. The DC bias voltage also allowed control of the kinetic energy (E_{Lab}) of ions in the laboratory frame. E_{Lab} is converted into the collision energy (E_{col}) between ions and reactant gas molecules in the center-of-mass frame using $E_{col} = E_{Lab} \times m_{neutral}/(m_{ion} + m_{neutral})$, where $m_{neutral}$ and m_{ion} are the masses of neutral and ionic reactants, respectively.

The ion beam intensities of CysH$^+$ and TrpH$^+$ were typically 4×10^5 and 5×10^5 ion/sec, respectively, and constant within 10%. Their initial kinetic energies were between 1.1 and 1.2 eV, and the energy spreads were around 0.4 eV which corresponds to an energy spread of ∼0.1 eV in the center-of-mass frame for the collision of CysH$^+$ (or TrpH$^+$) with $^1O_2$. Reaction cross sections were calculated from the ratio of product and reactant ion intensities, $^1O_2$ pressure, and the calibrated effective length of the scattering cell, using a Beer's Law relationship.[57]

$^1O_2$ was generated in a chemical generator using the following reaction[58,59]

$$H_2O_2 + Cl_2 + 2KOH$$
$$\rightarrow O_2(X^3{\textstyle\sum}_g{}^- \text{ and } a^1\Delta_g) + 2KCl + 2H_2O \qquad (1)$$
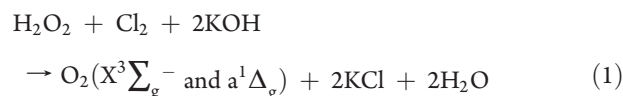
This $^1O_2$ generation technique was used to create oxygen−iodine lasers[60] and was introduced to ion−molecule reactions with $^1O_2$ by Viggiano and co-workers.[45,46,48−50] We adopted Viggiano et al.'s procedure with small modifications.[34]

In the experiment, 20 mL of 35 wt % H_2O_2 (Acros Organics) was very slowly mixed with 13 mL of 8.0 M KOH (>85%, Fisher) solution in a sparger that was immersed in a cold bath maintained at −19 °C. The resulting solution was held at −20 °C to lower the vapor pressure of the solution and prevent decomposition of H_2O_2, and was degassed before the reaction. A continuous flow of He (research grade, T. W. Smith) was introduced to the slushy H_2O_2/KOH mixture at a flow rate of 50 sccm to prevent freezing of the mixture at the exit of the fritted gas aerator inside the sparger. Cl_2 (≥99.5%, Sigma-Aldrich) was then added at a flow rate of 2−3 sccm. Cl_2 was mixed with He in a gas proportioner (Matheson model 7300) before bubbling through the H_2O_2/KOH solution. All the Cl_2 reacted to form ground-state and excited O_2.[46] The resulting gas mixture passed through a cold trap kept at −70 °C to remove the water vapor. Only ground-state O_2, $O_2(a^1\Delta_g)$ and He remained in the downstream gas flow and were introduced to ion−molecule collisions. Compared to the microwave discharge $^1O_2$ generator we used previously,[33] the chemical generator eliminated the O atom and ozone contaminants and produced a high yield of $^1O_2$. Before leaking into the scattering cell, the gases flowed through an emission cell to detect the emission of O_2 ($a^1\Delta_g \rightarrow X^3\Sigma_g^-$, $v = 0-0$) at 1270 nm.[61] The emission detection scheme has been described in a previous paper.[34] In brief, the emission cell was continuously pumped through a pressure control valve to maintain a pressure at 15 Torr. This pressure was chosen to reduce the residence time and hence, the wall quenching of $^1O_2$ inside the cold trap, gas tubing, and emission cell. Emission from the cell was collected by a plano-convex BK7 lens (f = 30 mm), and passed through an optical chopper (SRS model SR540) and a 0.5 nm bandwidth interference filter centered at 1270 nm (Andover, blocked to 1.55 μm). The chopped emission was focused by another plano-convex BK7 lens (f = 50 mm) into a thermoelectrically cooled InGaAs detector (Newport model 71887 detector and 77055 TE-cooler controller), and the signal was measured by a lock-in amplifier (SRS model SR830). Our detection system has not been calibrated, so we could not determine the absolute emission intensity. Since we adopted a very similar $^1O_2$ production procedure as Viggiano et al.'s, we assumed the maximum emission intensity detected corresponds to a 15% $^1O_2$ yield in the total oxygen flow as reported by Viggiano et al.[45,47,50] Since emission intensity linearly depends on $^1O_2$ concentration, the change of the $^1O_2$ yield during the experiment could be monitored by measuring the emission. $^1O_2$ pressure in the scattering cell is the product of the total gas pressure in the scattering cell, the percent of Cl_2 (assuming Cl_2 completely converted to O_2[46]) in the Cl_2/He flow, and the $^1O_2$ yield in the oxygen product. To check how reliable our determination of $^1O_2$ pressure in the scattering cell was, we measured the reaction cross section (σ_{Chem_O2}) of protonated tyrosine + $^1O_2$ using the same procedure just described, then compared it to our previous measurement (σ_{MW_O2}) which used a microwave discharge method to generate $^1O_2$, and the $^1O_2$ yield was estimated using the specific energy deposition per molecule during the discharge. A good agreement was found (i.e., $(\sigma_{Chem\_O2} - \sigma_{MW\_O2})/\sigma_{Chem\_O2}$ is within ∼35%), taking into account the combined errors in two experiments.

The collision cross section ($\sigma_{collision}$), taken as the greater of the ion-induced dipole capture cross section ($\sigma_{capture}$)[62] and hard-sphere collision cross section ($\sigma_{hard-sphere}$), is about 44−95 $Å^2$ for $CysH^+$ + O_2, and 60−95 $Å^2$ for $TrpH^+$ + O_2 in the studied E_{col} range of 0.05−1.0 eV. $\sigma_{hard-sphere}$ is calculated from the orientation-averaged contact radii of protonated amino acid and

O_2, and exceeds $\sigma_{capture}$ for $CysH^+$ + O_2 at E_{col} > 0.2 eV, and that for $TrpH^+$ + O_2 at E_{col} > 0.1 eV. The pressure of O_2/He in the scattering cell was maintained at 0.3−0.4 mTorr, which contained ∼5% of O_2. This pressure range was chosen to provide reasonable intensities of product ions, while keeping multiple-collision effects to a minimum level. In this range of pressure, the probability of $CysH^+$ and $TrpH^+$ undergoing a single-collision with O_2 is <3%, and that of double collisions is <0.1%. Note that $CysH^+$ and $TrpH^+$ also collided with He gas within the scattering cell, with a single-collision probability of 15−20%, and a double-collision probability of 3−6%. However, the light neutral-heavy ion combination makes these collisions insignificant compared to those with O_2.

Because the signals we measured are small, it is important to minimize systematic variation in experimental conditions that might be caused by drifting potentials, changes in ion beam intensities, $^1O_2$ yields, etc. The intensity of $^1O_2$ emission was monitored continuously during the whole experiment, and signal variation (controlled to be within 20%) was corrected for ion−molecule cross section. RPA measurements of primary ions were performed before and after each experiment to check the initial kinetic energy of the primary ion beam. As a check on reproducibility, the entire experiment was repeated several times and each time we cycled through different collision energies. The data presented are averages of several complete data sets. On the basis of the reproducibility of the cross section measurements taken over a two-month period, we estimate that the relative error is <20%. To check the reactivity of $CysH^+$ and $TrpH^+$ toward ground-state O_2 and He, control experiments were performed under the same conditions except that Cl_2 was replaced by oxygen gas at the same flow rate.

B. Computational Methods. To aid in reaction coordinate interpretation, density functional theory (DFT) electronic structure calculations were performed at the B3LYP/6-311++G(d, p) and B3LYP/aug-cc-pV5Z levels of theory, using Gaussian 09.[63] Note that due to the mixing of open-shell and closed-shell characteristics of $^1O_2$, standard DFT and MP2 methods lead to large errors in calculating the electronic excitation energy of $^1O_2$.[64] In our calculations, the DFT energy of $^1O_2$ was obtained by adding the experimental excitation energy of 0.98 eV[61] to the DFT energy of ground-state O_2. All geometries were optimized by calculating force constants at every step. Vibrational frequencies and zero-point energies (ZPE) were scaled by a factor of 0.955 and 0.981,[65] respectively. All the transition states (TSs) found were verified as first-order saddle points by frequency calculations, and the vibrational mode with the imaginary frequency corresponds to the reaction pathway. When necessary intrinsic reaction coordinate (IRC) calculations were used to determine which minima are connected by a particular TS. The details of the geometries for complexes, TSs, and products are available by request to the corresponding author.

To validate the importance of steps identified in the reaction coordinate for $CysH^+$ + $^1O_2$, quasi-classical, direct dynamics trajectory simulations were conducted. The chemical dynamics program VENUS99 of Hase et al.[66] was used to set up trajectory initial conditions, and the Hessian-based method of Bakken et al.[67] implemented in Gaussian was used to propagate each trajectory, with Hessians recalculated every five steps. Because millions of gradients and Hessian evaluations were required, the level of theory used for trajectories was necessarily modest. On the basis of the overall level of agreement with high level benchmark results and computational speed, we chose the

B3LYP method with 6−21G basis set for calculating trajectories. Trajectory integrations were performed with a step size of 0.25 amu$^{1/2}$ bohr (corresponding to a step size of ∼0.68 fsec in trajectory integrations), which conserved the total energy to better than 10^{-4} Hartree. The SCF = XQC option was adopted during trajectory integration so that a quadratically convergent Hartree−Fock (QC-SCF) method[63,68] was used in case the usual, but much faster, first-order SCF method did not converge within the allotted number of cycles.

The collision energy was set at 0.2 or 0.3 eV. For each collision energy, a batch of one hundred trajectories was calculated. The purpose of our trajectory simulations was to probe the gross features of the collisions between CysH$^+$ and $^1O_2$, thus both batches were calculated at impact parameter b = 0.1 Å, rather than randomly sampling the b distribution. For each trajectory batch, the initial conditions of the reactants were chosen to mimic the conditions of our experiment. Because CysH$^+$ ions were thermalized in the experiment, their initial vibrational and rotational energies were sampled from Boltzmann distributions at 300 K. Similarly, $^1O_2$ in the experiment was close to room temperature, so 300 K was used for both rotational and vibrational temperature for $^1O_2$. The quasi-classical initial vibrational state was simulated by giving each reactant atom displacement from equilibrium and momentum appropriate to the initial rovibrational state, with random phases for different modes. Both CysH$^+$ and $^1O_2$ have zero-point energy in all vibrational modes. Randomly oriented CysH$^+$ and $^1O_2$ were given relative velocities corresponding to the simulated collision energy. All trajectories started with an initial center-of-mass reactant separation of 7.0 Å, and were terminated either when the distance between the final products exceeded 9.0 Å, or after 5000 steps. The error in the energy due to the long-range potential at 7.0 Å is less than 8 meV. Trajectories were calculated on an Intel core 2 duo and core 2 quad (3.0 GHz) based 64 bit Linux computational cluster, and each trajectory took ∼240 CPU hours. For trajectory visualization we used the program gOpenMol.[69] Analysis of individual trajectories and statistical analysis of the trajectory ensemble was done with programs written for this purpose, as described previously.[70−72]

III. RESULTS AND DISCUSSION

A. Reaction Cross Sections. For the reaction of CysH$^+$ (m/z 122) + $^1O_2$, product ions were observed at m/z 74 over the collision energy range of 0.05−0.75 eV, corresponding to a structure of H$_2$NCHCO$_2$H$^+$. At high collision energies, product ions were also observed at m/z 105, 76, and 18. The latter three product ion masses correspond to the elimination of NH$_3$, H$_2$O + CO and NH$_4^+$ from CysH$^+$, respectively. [CysH$^+$−NH$_3$], [CysH$^+$ − (H$_2$O + CO)] and NH$_4^+$ are attributed to collision-induced dissociation (CID),[73−77] and were observed upon collisions with ground-state O$_2$ and He, too. There is no sign of elimination involving the sulfhydryl group or H$_2$S. Among three CID product channels, [CysH$^+$ − NH$_3$] and NH$_4^+$ are largely dominant, while [CysH$^+$ − (H$_2$O + CO)] increases in importance with increasing collision energy. Product ions of H$_2$NCHCO$_2$H$^+$, on the other hand, were not observed with ground-state O$_2$ or He, and cannot be attributed to a CID product.

The cross section of H$_2$NCHCO$_2$H$^+$ production is shown in Figure 1 over the E_{col} range from 0.05 to 0.75 eV. Also shown in the figure is the reaction efficiency (right-hand scale), calculated
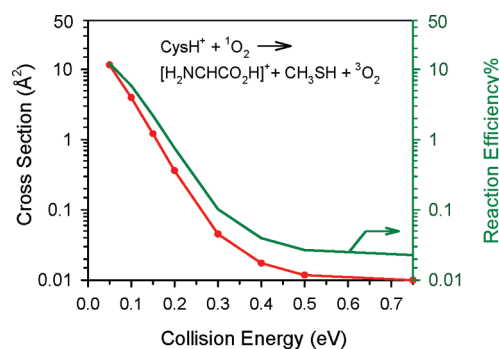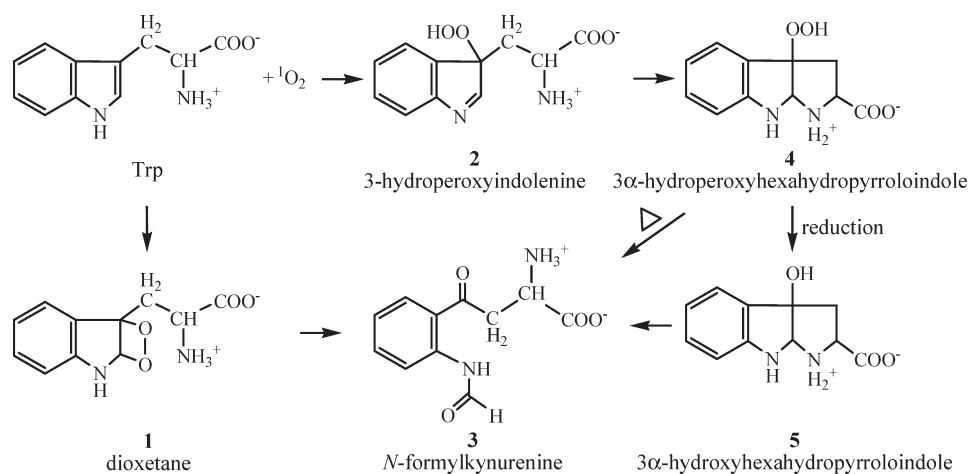

Figure 1. Cross section for the reaction of CysH$^+$ with $^1O_2$, as a function of center-of-mass collision energy. Also shown is the estimated reaction efficiency.
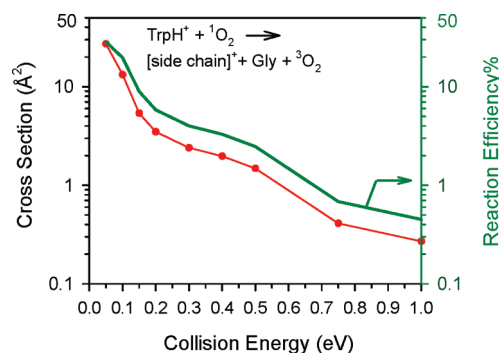
Figure 2. Cross section for the reaction of TrpH$^+$ with $^1O_2$, as a function of center-of-mass collision energy. Also shown is the estimated reaction efficiency.

by $\sigma_{reaction}/\sigma_{collision}$. Note that the absolute values of cross sections were calculated on the basis of the assumption that the maximum $^1O_2$ yield from the chemical $^1O_2$ generator is 15%;[45,47,50] there may, therefore, exist uncertainty concerning absolute cross sections. However, based on our previous experiment of protonated methionine (MetH$^+$) with $^1O_2$, we tend to believe that the absolute uncertainty is around ±35%.[34] More importantly, this source of uncertainty would not affect the relative cross sections, i.e., the collision energy dependence of cross section, which is the primary interest in the study. In our ion scattering experiments,[33,34] an uncertainty of 20% was quoted for relative cross sections. The reaction cross section of CysH$^+$ + $^1O_2$ is significant only at the lowest energies, and is strongly inhibited by collision energy, becoming negligible at $E_{col} \geq$ 0.5 eV. The reaction is inefficient even at the lowest E_{col}. The reaction efficiency is ∼12% at E_{col} = 0.05 eV, drops to less than 1% at E_{col} = 0.2 eV. This behavior suggests that the reaction might be mediated by a complex, with complex formation probability and/or lifetime that are strongly suppressed by collision energy.
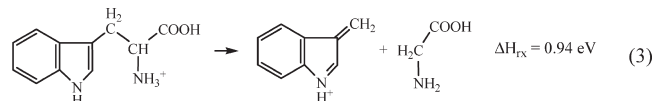
For the reaction of TrpH$^+$ (m/z 205) with $^1O_2$, product ions were observed at m/z 130, corresponding to the formation of a charged aromatic indole side chain. In addition, CID products were observed at m/z 188 and 159 at high collision energies, corresponding to the elimination of NH$_3$ and H$_2$O + CO from TrpH$^+$, respectively.[73,75,77−80] These CID products were also observed in the control experiments with ground-state O$_2$ and He, and therefore are not relevant to $^1O_2$ chemistry. In contrast, product ions of m/z 130 were only produced with $^1O_2$. The cross

Figure 3. Reaction paths for photooxidation of Trp in solution.

section for the product channel of m/z 130 is shown in Figure 2 over the center-of-mass E_{col} range from 0.05 to 1.0 eV, together with the reaction efficiency estimated as in the case of CysH$^+$+ ^{1}O$_2$. The reaction appears to be exothermic without having any energy barriers above the reactants. The reaction cross section declines with E_{col}, and the reaction efficiency drops from 28% at E_{col} = 0.05 eV to 6% at 0.2 eV, and to less than 1% at 0.75 eV and greater.

Since H$_2$NCHCO$_2$H$^+$ and Trp side chain cation are the only product ions specific to ^{1}O$_2$ reactions, we will focus on these two product channels in the following discussion. Assuming that H$_2$NCHCO$_2$H$^+$ and Trp side chain cation were produced from unimolecular dissociation of CysH$^+$ and TrpH$^+$, respectively, the dissociation energies are as follows:

$$H_3NCH(CO_2H)CH_2SH^+ \rightarrow H_2NCHCO_2H^+ + CH_3SH \qquad \Delta H_{rx} = 1.09 \text{ eV} \qquad (2)$$


$$\Delta H_{rx} = 0.94 \text{ eV} \qquad (3)$$

Listed energetics are calculated at B3LYP/aug-cc-pV5Z for CysH$^+$ and B3LYP/6-311++G(d, p) for TrpH$^+$, respectively. We tested the effects of the basis set on CysH$^+$ dissociation. The extension of the basis set up to aug-cc-pV5Z lowers the dissociation energy by 0.1 eV as compared to the 6-311++G(d, p) basis set. As will be discussed below, both reactions involve intramolecular transfer of a H atom prior to (or concurring with) C$^\alpha$–C$^\beta$ bond cleavage of the corresponding amino acid. For CysH$^+$, the intramolecular H atom transfer occurs from the ammonium group to the C$^\beta$ atom; and for TrpH$^+$, from the ammonium group to the C$^\alpha$ atom. Clearly, dissociation of CysH$^+$ and TrpH$^+$ must be prompted by the electronic excitation energy of ^{1}O$_2$. To realize this electronic energy transfer, a strong interaction is needed to affect the electronic property of ^{1}O$_2$ and thus break the spin conservation propensity rule. Otherwise, dissociation could not happen at low E_{col}. Instead, we would have observed endothermic collision energy dependence of the cross sections for producing H$_2$NCHCO$_2$H$^+$ and Trp side chain cation, i.e., the cross section rises from zero at an appearance energy near the dissociation threshold, increases rapidly with E_{col}, and eventually approaches the hard-sphere collision cross section.[81]

Note that Viggiano et al. reported several examples in which the electronic excitation energy of ^{1}O$_2$ can be utilized for driving endothermic reactions, such as endothermic electron transfer with anions O$_2^-$, SO$_2^-$, and HO$_2^-$.[45,47] Recently, they reported that in the reactions of ^{1}O$_2$ with OH$^-$(H$_2$O)$_{1,2}$ clusters, where the energies for dissociating one hydroxide-water bond are of the order of the electronic excitation energy of ^{1}O$_2$, ^{1}O$_2$ can devote its excitation energy to dissociating OH$^-$(H$_2$O)$_{1,2}$,[48] the so-called dissociative excitation transfer. Their study indicated that dissociative excitation transfer of ^{1}O$_2$ with OH$^-$(H$_2$O)$_1$ is slightly endothermic, but becomes exothermic with OH$^-$(H$_2$O)$_2$.

B. Comparison with Solution-Phase Photooxidation Results. Before we discuss the reaction mechanisms of CysH$^+$ and TrpH$^+$ with ^{1}O$_2$, it is useful to review the photooxidation results of Cys and Trp in solution. The ease of oxidation of the S atom makes Cys very reactive in photosensitized oxidation reactions. Reactions involve both Type I (i.e., radical-mediated) and Type II (i.e., ^{1}O$_2$-mediated) processes, and show strong pH dependence.[20−26] ^{1}O$_2$-mediated process is important at high pH (8 to 11), while radical-mediated process occurs at low pH (4 to 6). Cystine is the major product at both high and low pH values. The reaction that gives rise to cystine may involve a persulfoxide intermediate though the mechanism remains obscure. This reaction is in fact biologically relevant because that controlled oxidation of Cys residues and reduction of cystine residues constitute a redox switching mechanism that controls the structure and function of a number of key proteins.[10,82] In addition to cystine, oxidation products include oxyacids (RSO$_2$H and RSO$_3$H) and other species that remain to be fully elucidated.

^{1}O$_2$-meditaed photooxidation of Trp involves multiple steps and various intermediates.[14,27−32] Reaction initially yields a dioxetane intermediate **1** across the C2—C3 double bond on the indole side chain; alternatively, the reaction can form an energetically more favorable intermediate 3-hydroperoxyindolenine **2**. Subsequent C2—C3 bond cleavage of **1** yields N-formylkynurenine **3**. **2** undergoes an intramolecular addition to form 3α-hydroperoxyhexahydropyrroloindole **4**, followed by rearrangement to **3** on warming or reduction to 3α-hydroxyhexahydropyrroloindole **5**. Decomposition of **5** also results in **3**. These reaction pathways are depicted in Figure 3. Different than Cys, Trp gives rise to significant physical quenching of ^{1}O$_2$ in addition to chemical reactions.[83,84] These solution-phase results provide us a guide for the construction of gas-phase reaction coordinates in the next section.
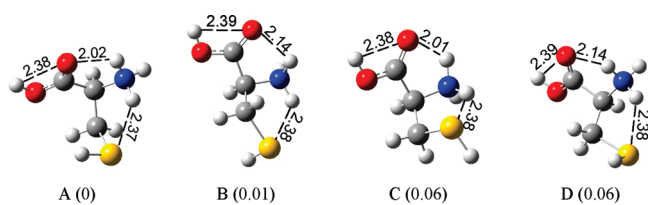
Figure 4. Low-lying conformations of CysH$^+$ calculated at B3LYP/6-311++G(d, p). Their relative energies at 0 K (eV, including ZPE) are indicated in parentheses. The distances are shown in angstroms.
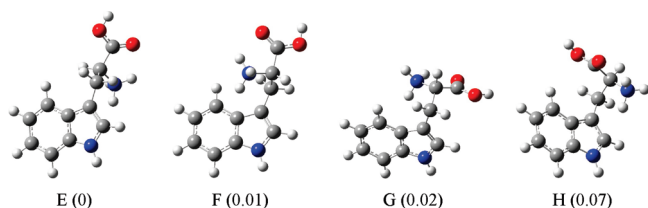
Figure 5. Low-lying conformations of TrpH$^+$ calculated at B3LYP/6-311++G(d, p). Their relative energies at 0 K (eV, including ZPE) are indicated in parentheses.

C. Reaction Mechanisms. CysH$^+$ and TrpH$^+$ may exist in various geometric conformations resulting from the flexibility of their structures. To find the global minima of their conformational landscape, we applied a grid search method.[85] Since we are only interested in low-energy conformations, we assumed a *syn*-configuration of the carboxylic acid group and a bifurcated H$_2$NH$^+$···O=C intramolecular hydrogen bond in both CysH$^+$ and TrpH$^+$. Furthermore, based on literature we assumed that the α-amino nitrogen is the most favorable protonation site for both amino acids.[79,86,87] Note that Rogalewicz et al.[77] reported the absence of immonium fragment ion (i.e., concomitant loss of H$_2$O + CO) in the CID of TrpH$^+$. They rationalized the result by a high proton affinity of the Trp amino terminus, and took this as a manifestation that TrpH$^+$ was initially protonated on the indole nitrogen atom. However, this result seems in disagreement with TrpH$^+$ CID results of other groups.[73,75,78] The suggestion of side chain protonation also contradicts with computational studies which confirmed protonation on the α-amino nitrogen of Trp.[79,86]

We systematically rotated each of the torsion angles along the amino acid side chain through 360° at 60° increments to generate all possible conformations of CysH$^+$ and TrpH$^+$, the so-called rotamers. Every conformation so generated was subjected to geometry optimization at the B3LYP/6-31+G* level of theory to derive the associated minimum energy conformations. Many of the initial conformations were optimized to the same minimum energy structure. These conformations were then optimized at the B3LYP/6-311++G(d, p) level of theory. Their structures and relative energies at 0 K (including ZPE) are summarized in Figures 4 and 5.

Four lowest energy conformations (within 0.1 eV) were found for each of CysH$^+$ and TrpH$^+$, respectively. The low-lying conformations for CysH$^+$, A−D in Figure 4, have strong intramolecular C=O ← NH$_3^+$ →S charge complexation and hydrogen bond interactions, with a distances of 2.37−2.38 Å between the S atom and the closest H atom of the ammonium group, and a distance of 2.01−2.14 Å between the carbonyl O atom and the closest H atom of the ammonium group. In addition, there exists a hydrogen bond between the carbonyl O atom and

the hydroxyl H atom with a distance of 2.38−2.39 Å. The next group of stable conformations, with weak NH$_3^+$ →S interactions, lies 0.28−0.33 eV higher in energy with respect to A, and is less likely to be populated at experimental temperature of 300 K. According to the infrared multiphoton dissociation spectroscopy (IRMPD) measurement by Armentrout and co-workers,[88] a mixture of conformations A−D accounts for the population of CysH$^+$ at room temperature.

A set of low-lying conformations of TrpH$^+$, E−H, is depicted in Figure 5. All conformations have the ammonium group pointing to or located above the aromatic indole ring. These conformations are stabilized by a hydrogen bond between the ammonium H atom and the carbonyl O atom, and another hydrogen bond between the ammonium H atom and the π-system of the indole side chain. Our lowest energy conformations of TrpH$^+$ are consistent with previous calculations carried out at B3LYP/6-31G*,[79] B3LYP/6-31+G*,[89] and MP2/SV(P) levels of theory,[90,91] and the IRMPD spectroscopy of TrpH$^+$ by Mino et al.[89] The next group of conformations with the ammonium group away from the indole ring has energy more than 0.30 eV higher than E.

Our subsequent calculations of the reaction coordinates for CysH$^+$ + ^{1}O$_2$ and TrpH$^+$ + ^{1}O$_2$ focused on the lowest energy conformations, i.e., A for CysH$^+$ and E for TrpH$^+$. It is certainly possible that interconversion between different rotamers A−D, and between E−H might occur during collisions. However, it seems less likely that different conformations of CysH$^+$ and TrpH$^+$ would significantly alter their reaction coordinates, as confirmed in our previous trajectory simulations of TyrH$^+$ + ^{1}O$_2$[33] and MetH$^+$ + ^{1}O$_2$.[34]

1. CysH$^+$ + ^{1}O$_2$.

1.1. Direct Sequential vs Complex-Mediated Mechanism. As discussed above, the reaction of CysH$^+$ + ^{1}O$_2$ has to be driven by the excitation energy of ^{1}O$_2$. A related question arises to the nature of energy transfer from ^{1}O$_2$. One can imagine two mechanisms for dissociation of CysH$^+$ to H$_2$NCHCO$_2$H$^+$. The reaction of CysH$^+$ + ^{1}O$_2$ could proceed in a direct sequential mechanism as invoked in conventional CID. By this we mean an activating collision where the excitation energy of ^{1}O$_2$ and a fraction of collision energy are converted to internal energy of CysH$^+$, followed by unimolecular decomposition of excited CysH^{+*} after O$_2$ has recoiled. However, such direct sequential mechanism could be ruled out for CysH$^+$ + ^{1}O$_2$ for several reasons. First, a direct collision would likely show E_{col} enhancement rather than inhibition for an endoergic reaction (i.e., reaction 2), since T → E$_{internal}$ conversion is helpful for overcoming the reaction threshold as we observed in typical CID reactions.[72,81] Second, since the excitation energy of the triplet excited state of CysH$^+$ is calculated to be 4.17 eV, the electronic energy transfer from ^{1}O$_2$ to ^{3}CysH$^+$ (via intersystem crossing) is not feasible. Energy transfer from ^{1}O$_2$ to CysH$^+$ may arise via electronic to vibrational energy conversion,[92] and produce vibrationally excited CysH^{+*} which is capable of predissociation. But predissociation of CysH^{+*} cannot explain the intramolecular H atom transfer observed in our measurement. Direct C^α−C^β bond cleavage of vibrationally excited CysH^{+*} would most likely produce H$_3$NCHCO$_2$H$^+$ (m/z 75) + CH$_2$SH or H$_3$NCHCO$_2$H + CH$_2$SH$^+$ (m/z 47). These two pairs of products only differ in the charge states. Their thresholds amount to 3.5 and 3.8 eV, respectively, too far above the ^{1}O$_2$ excitation energy. As a result, only CID product ions of CysH$^+$, i.e., m/z 105, 76, and 18, would be expected for the direct sequential process should it occur.

The alternative reaction mechanism for CysH$^+$ + ^{1}O$_2$ involves formation of a complex between CysH$^+$ and ^{1}O$_2$, and the
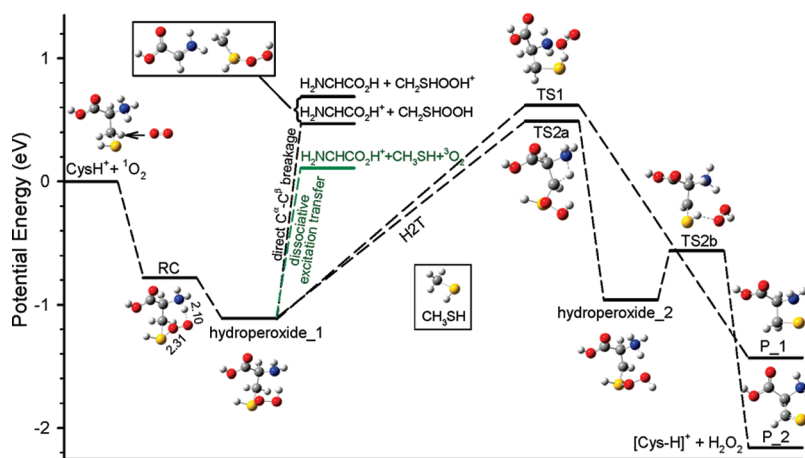
Figure 6. Schematic reaction coordinate for $CysH^+ + {}^1O_2$. Energies of complexes, TSs, and products, relative to reactants, are derived from a combination of B3LYP/6-311++G(d, p) and B3LYP/aug-cc-pV5Z results, including ZPE. The bond distances are shown in angstroms.

electronic energy of $^1O_2$ converts into whatever form of internal energy needed for dissociating the complex. The dissociation must be concerted; i.e., O_2 must remain in close proximity to $CysH^+$ as $CysH^+$ dissociates; in the meantime, strong spin–orbital coupling within the complex could "catalyze" access to the triplet channel with no activation energy in excess of the asymptotic energy for the products. A similar concerted mechanism has been reported for a spin-forbidden CID reaction of NO_2^+ $({}^1\Sigma_g^+) + Xe \rightarrow NO^+({}^1\Sigma_g) + O({}^3P) + Xe$.[72] A complex-mediated mechanism is reasonable for a system like $CysH^+ + {}^1O_2$, since the number of degrees of freedom is large and the interaction between $CysH^+$ and $^1O_2$ is strong. In addition, the observed E_{col} dependence for $CysH^+ + {}^1O_2$ is consistent with a complex-mediated mechanism. A final point in this regard is that production of $H_2NCHCO_2H^+ + CH_3SH$ requires intramolecular H atom transfer—further evidence that reinforces a complex-mediated mechanism.

1.2. Reaction Coordinate. DFT calculation results for the complex-mediated reaction coordinate of $CysH^+ + {}^1O_2$ are summarized in Figure 6, with the reactants shown at zero energy. Energetics are derived from a combination of B3LYP/6-311++G(d, p), B3LYP/aug-cc-pV5Z results and the experimental value of $^1O_2$ excitation energy. One weakly bound complex (RC) and one covalently bound complex (hydroperoxide_1) were identified. Complex RC can be characterized as a reactant-like complex, formed by electrostatic interaction and ionic hydrogen bond. This complex has O_2 moiety sandwiched between the NH_3^+ group and the S atom of $CysH^+$, with distances of 2.31 and 2.10 Å for $S\cdots O-O$ and $O-O\cdots HNH_2^+$, respectively. The binding energy of RC is 0.78 eV with respect to the reactants. Because no rearrangement is needed to form a reactant-like complex from the reactants, it is less likely to have significant barriers inhibiting the formation of this complex. This was verified in a relaxed potential energy surface (PES) scan running along the dissociation of RC back to the reactants, as well as the direct dynamics trajectory simulations discussed below. Because of a lack of directional covalent bonds between $CysH^+$ and O_2, complex RC does not have a well-defined geometry at the energies available in our experiment, and is rather floppy with a large amplitude of intermolecular motion. The significance of complex RC is that it allows repeated encounters between reactants, which may eventually lead to the formation of hydroperoxide_1. To this extent, complex RC acts as a "precursor complex".

Hydroperoxide_1 is a covalently bound intermediate, with a binding energy of 1.11 eV. According to the Mulliken charge population analysis, the $-SOOH$ group carries most of the positive charge ($\delta^+ = 0.74$). This is partly because the persulfoxide group has a higher proton affinity and partly because that more efficient hydrogen bonding and charge complexation are allowable through a seven-membered ring of $[-C-C-SOO-NH-]$ formed in hydroperoxide_1. This exemplifies that an oxidation-induced post-translational modification may change the protonation site of an amino acid. A similar phenomena has been found for $MetH^+ + {}^1O_2$.[34] As proved by a relaxed PES scan running along the OH distance of $O-O\cdots HNH_2^+$, there is no activation barrier for interconversion between precursor complex RC and hydroperoxide_1.

It is interesting to note that at the early stage of the reaction, $CysH^+ + {}^1O_2$ shows identical behavior as that of $MetH^+ + {}^1O_2$.[34] Both $CysH^+$ and $MetH^+$ form precursor complexes upon collisions with $^1O_2$, and both of which interconvert to covalently bound hydroperoxides. For $MetH^+ + {}^1O_2$, the hydroperoxide undergoes interconversion to another hydroperoxide where the hydroperoxide group rotates away from the amino group. The formed hydroperoxide is followed by elimination of H_2O_2. The overall reaction of $MetH^+ + {}^1O_2$ thus corresponds to generation of H_2O_2 via transfer of two H atoms from $MetH^+$ to $^1O_2$, i.e., H2T reaction. On the basis of the resemblances between $CysH^+$ and $MetH^+$ (in terms of reactant structures and their complexes with $^1O_2$), we had expected to observe a H2T reaction for $CysH^+ + {}^1O_2$. Figure 6 shows the possible H2T reaction pathways for $CysH^+ + {}^1O_2$ at low collision energies. Hydroperoxide_1 may eliminate H_2O_2 via concerted elimination of -OOH and the H atom of the sulfhydryl group, producing product ion P_1 (i.e., $H_2NCH(CO_2H)CH_2S^+$) at m/z 120; however, this H2T pathway bears an activation barrier TS1 (0.62 eV above the reactants). Alternatively, hydroperoxide_1 may interconvert to hydroperoxide_2 via TS2a (0.49 eV above the reactants), which is followed by elimination of H_2O_2 via TS2b (0.40 eV above hydroperoxide_2) to form product ion P_2 (i.e., $H_3NCH(CO_2H)CHS^+$), also at m/z 120. Nevertheless, neither of these H2T pathways can open at low collision energies. Accordingly, no H2T products were observed for $CysH^+ + {}^1O_2$.

This raises a question regarding the fate of hydroperoxide_1. On the basis of DFT calculation results, hydroperoxide_1 may
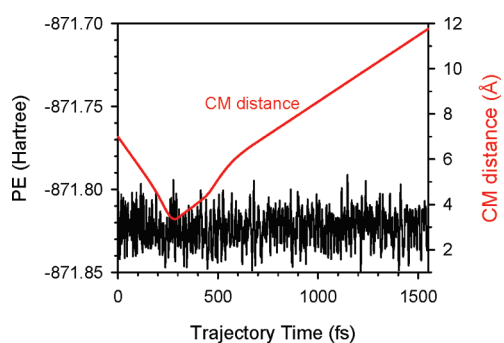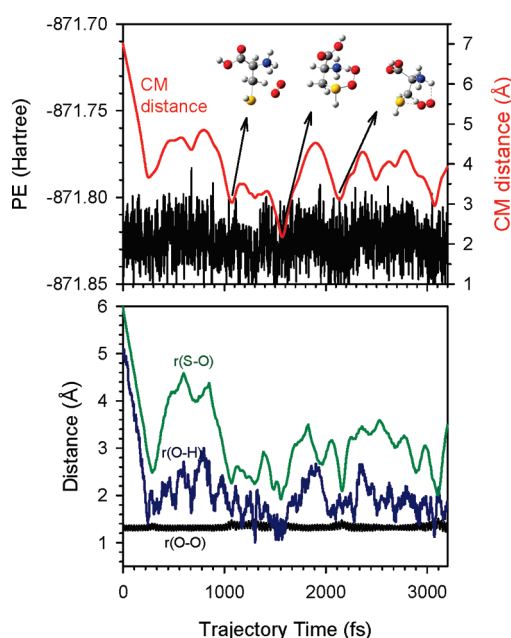
Figure 7. Representative plot of nonreactive trajectories at E_{col} = 0.2 eV, showing the variation of potential energy and center-of-mass distance between CysH$^+$ and O$_2$ moieties during the trajectory.

dissociate, via direct cleavage of the C$^\alpha$—C$^\beta$ bond, to two pairs of products which only differ in which fragment carries charge, i.e., NH$_2$CHCO$_2$H$^+$ (m/z 74) + CH$_2$SHOOH and NH$_2$CHCO$_2$H + CH$_2$SHOOH$^+$ (m/z 80). Their dissociation energies are calculated to be 0.45 and 0.69 eV (without taking into account any possible barriers above the product asymptotic limits), respectively. Therefore, these dissociation channels would not occur at low energies. Hydroperoxide_1 must seek a more energetically favorable dissociation path to NH$_2$CHCO$_2$H$^+$.

Recently, Viggiano et al. proposed a dissociative excitation transfer mechanism for the reactions of OH$^-$(H$_2$O)$_{1,2}$ with ^{1}O$_2$,[48] where ^{1}O$_2$ devotes the electronic excitation energy to dissociating OH$^-$(H$_2$O)$_{1,2}$, and itself decays to ground-state O$_2$. Here we propose a similar mechanism for CysH$^+$ + ^{1}O$_2$. In the reaction, hydroperoxide_1 undergoes three-body dissociation to H$_2$NCHCO$_2$H$^+$, CH$_3$SH, and ground-state O$_2$. Intramolecular H atom transfer occurs simultaneously with dissociation of hydroperoxide_1, transferring the H atom of —SOOH to the C$^\beta$ atom of CysH$^+$. Assuming all of the ^{1}O$_2$ excitation energy could be used to drive the dissociation of hydroperoxide_1, the calculated ΔH_{rx} is 0.11 eV, as indicated by the green line in Figure 6. This reaction endoergicity is comparable to the E_{col} broadening ($\sim$0.1 eV) resulting from the distributions of ion beam and target molecule velocities in our experiment. In other words, at the lowest nominal E_{col} a large fraction of collisions has energy more than the threshold energy, and can react. As a result, the reaction cross section generally increases with decreasing E_{col}, presenting "exothermic" reaction patterns. Similar E_{col} dependence has been reported for an endothermic reaction of H$_2$CO$^+$ + OCS → OCSH$^+$ + HCO, with a threshold energy between 0.04 to 0.22 eV.[93]

1.3. Direct Dynamics Trajectory Simulations. Whether or not hydroperoxide_1 is important for the reaction also hinges on the extent to which hydroperoxide_1 forms during collisions of CysH$^+$ + ^{1}O$_2$. To explore this issue, we conducted direct dynamics trajectory simulations for CysH$^+$ + ^{1}O$_2$ at E_{col} = 0.2 and 0.3 eV. The quasi-classical trajectory method we used is not applicable to nonadiabatic collisions, i.e., it does not allow transitions from a singlet to a triplet state. Therefore, trajectories cannot reproduce the "spin-forbidden" dissociative excitation transfer. However, analysis of trajectories provides information concerning the early time dynamics where the electron spin of the reactants remains conserved. Figures 7 and 8 illustrate trajectories representative of nonreactive and reactive collisions at E_{col} = 0.2 eV, respectively. Both figures show changes of various distances and potential energy during the trajectory. The CM


Figure 8. Representative plot of complex-forming trajectories at E_{col} = 0.2 eV: (top) the variation of potential energy and center-of-mass distance between CysH$^+$ and O$_2$ moieties during the trajectory and (bottom) the variation of various bond lengths during the trajectory.

distance is the distance between the centers of mass of the collision partners. Figure 7 shows a direct, nonreactive scattering, with only one turning point in the relative motion of reactant centers of mass; i.e., there is no sign of mediation by a complex in this collision. The time scale of the collision is somewhat arbitrary, but three numbers are relevant. The time between the start of trajectory and the onset of strong interaction, which depends on collision orientation, is around 0.25 ps. The time for reactants approach within 5 Å is around 0.35 ps. And the time period during which CysH$^+$ and ^{1}O$_2$ are interacting strongly is around 0.1 ps, as shown by the potential energy spike beginning at t = 0.25 ps during the trajectory. During the trajectory, potential energy fluctuates due to vibrational motions of the reactants. Figure 8 demonstrates a complex-forming trajectory, with similar reactants approach time. No obvious potential barrier was observed during the reactive collision. The r(S—O) and r(O—H) distances plotted in the figure correspond to the lengths of S-OO and SOO-H bonds being formed in the complex, and r(O—O) is the bond length of the O$_2$ moiety. The high frequency oscillations of r(S—O), r(O—H), and r(O—O) reflect the vibrations of the reactants or products, including ZPE. The large-amplitude, low frequency oscillations of r(S—O) and r(O—H) reflect the interconversion between precursor complex RC and covalently bond hydroperoxide_1, as shown in the snapshots inserted in Figure 8, as well as the molecular rotations.

At E_{col} = 0.2 eV and b = 0.1 Å, roughly 55% of all trajectories formed complexes (either precursor complex RC or hydroperoxide_1), and the remaining trajectories belong to direct, nonreactive scattering. At E_{col} = 0.3 eV, the probability of forming a complex during the trajectory decreases to 40%. It is interesting to note that the formation of complex is collision orientation dependent. Almost all complex-forming trajectories have O$_2$ approach both the S atom and the ammonium group of CysH$^+$ simultaneously when the reactants start to collide. The collisions, with O$_2$ either attack the backbone of CysH$^+$ or approach the
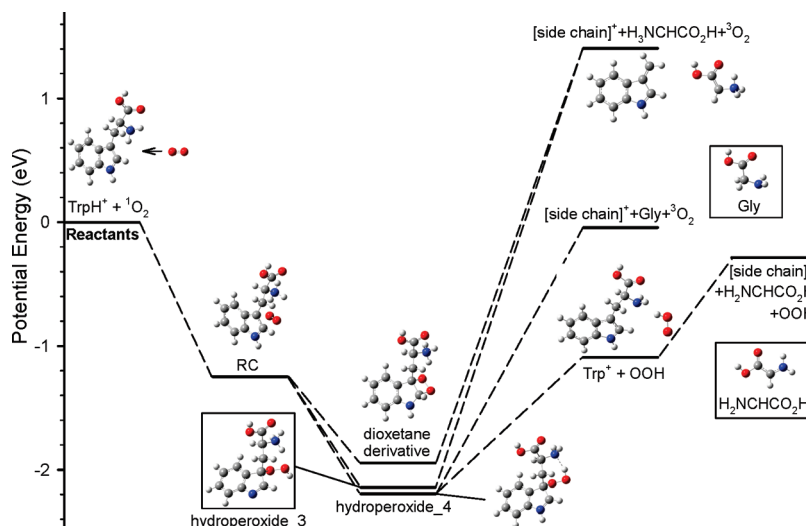
Figure 9. Schematic reaction coordinate for $TrpH^+ + {}^1O_2$. Energies of complexes, TSs, and products, relative to reactants, are derived from B3LYP/6-311++G(d, p) values, including ZPE.
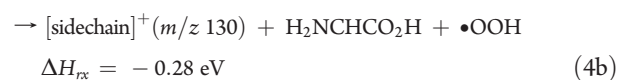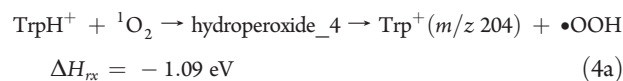
sulfhydryl group from the back side of the ammonium group, mostly lead to nonreactive scattering. Similar phenomena were observed in the trajectories of $MetH^+ + {}^1O_2$.[34] The narrow range of optimal orientations could to some extent account for the low reaction efficiency observed for $CysH^+ + {}^1O_2$. Note the spin-forbidden process could impose other dynamics bottlenecks for reaction; however, detailed theoretical calculations are needed for the evaluation of this effect.

Of all complex-forming trajectories, only less than half decay back to the reactants before the termination of the trajectory (~3.4 ps). This suggests that the lifetime of most precursor complex and hydroperoxide_1 is longer than 3 ps. For comparison, the classical rotational period of a complex estimated using the average angular momentum varies from 1.9 to 2.1 ps at $E_{col} = 0.2-0.3$ eV. We also estimated the direct "fly by" time, taken as the time required for 5 Å motion at the relative speed of reactants. This gives a measure of how long a direct collision would last at the same collision energy. This "fly by" time is 0.4 ps at $E_{col} = 0.2$ eV, drops to 0.33 ps at $E_{col} = 0.3$ eV. The complex lifetime is thus significantly longer than "fly by" times, and comparable to complex rotational periods. Besides, the trajectories show correct E_{col} dependence in terms of the complex formation probability, i.e., 55% at 0.2 eV vs 40% at 0.3 eV. The conclusion is that precursor complex RC and hydroperoxide_1 would be able to mediate the reaction at low E_{col}.

2. $TrpH^+ + {}^1O_2$. DFT calculated reaction coordinate for $TrpH^+ + {}^1O_2$ is summarized in Figure 9. The electronic excitation energy of the lowest ${}^3TrpH^+$ is 1.83 eV higher than that of ${}^1O_2$; therefore, as in the case of $CysH^+ + {}^1O_2$, we need not consider the participation of electronically excited $TrpH^+$ in the reaction. One weakly bound, reactant-like complex and three strongly bound complexes were found that might be important in mediating the reaction. To differentiate the reactant-like complexes for $CysH^+ + {}^1O_2$ and $TrpH^+ + {}^1O_2$, we include the reactant formula in the acronym, e.g., $RC(TrpH^+)$, for clarity. Complex $RC(TrpH^+)$, analogous to complex $RC(CysH^+)$ for $CysH^+ + {}^1O_2$, has the O_2 moiety interacting with the ammonium group via hydrogen bonding and the indole side chain via electrostatic interaction. $RC(TrpH^+)$ is calculated to have a binding energy of 1.25 eV relative to the reactants, more strongly

bound than in the $CysH^+ + {}^1O_2$ system. Consistent with the reaction mechanism proposed for solution-phase photooxidation of tryptophan (see Figure 3), $RC(TrpH^+)$ could interconvert to a dioxetane derivative across the C2—C3 double bond on the indole side chain, or form a hydroperoxide at C3. In the dioxetane intermediate, two affected carbon atoms are slightly displaced from the ring plane toward O_2. Two structures were identified for hydroperoxide complex, i.e., hydroperoxide_3 and hydroperoxide_4 with the difference being which H atom is abstracted by the peroxide group. In hydroperoxide_3, the H atom of the indole —NH is abstracted; while in hydroperoxide_4, one H of the ammonium group is transferred to the peroxide group. Consequently, in hydroperoxide_3, the charge stays on the ammonium group; while in hydroperoxide_4, the charge shifts to the side chain and is shared by the indole ring ($\delta^+ = 0.61$) and the hydroperoxyl group ($\delta^+ = 0.31$). The binding energies are 1.94 eV for dioxetane, 2.14 eV for hydroperoxide_3, and 2.19 eV for hydroperoxide_4, all calculated with respect to the reactants.

Product ions of m/z 130 are barely observed in CID of $TrpH^+$, but they are the major fragmentation channel in photoinduced dissociation of $TrpH^+$.[94−97] In photodissociation of $TrpH^+$, m/z 130 can be produced either through prompt $C^\alpha-C^\beta$ bond breaking of electronically excited $TrpH^{+*}$, or from a two-step mechanism.[94−97] In the two-step mechanism, photoexcitation leads to a H atom loss reaction, and the hence formed radical cation Trp^+ (m/z 204) further dissociates into its specific m/z 130 fragment by $C^\alpha-C^\beta$ bond rupture. As discussed above, electronically excited $TrpH^{+*}$ can be excluded in our reaction based on energetics consideration, thus we need to only consider the possibility of a two-step mechanism for $TrpH^+ + {}^1O_2$, i.e., Trp^+ is produced by a H atom abstraction of $TrpH^+$ by ${}^1O_2$ (reaction 4a) followed by dissociation of Trp^+ to m/z 130 (reaction 4b). The reaction energetics, calculated at the B3LYP/6-311++G(d, p) level of theory, are as follows:

$$TrpH^+ + {}^1O_2 \rightarrow \text{hydroperoxide\_4} \rightarrow Trp^+(m/z\ 204) + \bullet OOH$$

$$\Delta H_{rx} = -1.09 \text{ eV} \tag{4a}$$

$$\rightarrow [\text{sidechain}]^+(m/z\ 130) + H_2NCHCO_2H + \bullet OOH$$

$$\Delta H_{rx} = -0.28 \text{ eV} \tag{4b}$$

The enthalpy of reaction 4a, 1.09 eV, has to distribute into the internal modes and recoil energies of both fragments, and only a faction of exoergicity should be left in the nascent Trp$^+$ radical cation. On the other hand, assuming a direct, barrier free mechanism, the dissociation energy of Trp$^+$ is calculated to be 0.81 eV. Because of the internal energy distribution in the nascent Trp$^+$ ions, one can image that not all of these Trp$^+$ ions would be able to carry sufficient internal energy for $C^\alpha - C^\beta$ bond cleavage; consequently, parent Trp$^+$ (m/z 204) and fragment (m/z 130) ions would be detected simultaneously as product ions should the dissociation pathway of 4a and 4b open. However, we did not observe noticeable signal at m/z 204 beyond the background. Therefore, product ions of m/z 130 cannot come from the fragmentation of Trp$^+$ in our reaction.

In Figure 9, we have attempted to identify three possible pathways leading to the transfer of the electronic excitation energy of $^1O_2$ and formation of m/z 130, each of these is mediated by a dioxetane or a hydroperoxide. Dioxetane could dissociate into charged side chain, neutral H$_3$NCHCO$_2$H, and ground-state O$_2$. The same dissociation products could be expected for hydroperoxide_3, and in that case the H atom of the hydroperoxyl group transfers back to the indole N. However, the enthalpy of reaction corresponding to these dissociation products is calculated to be 1.41 eV endothermic, suggesting that neither of dioxetane and hydroperoxide_3 is a good candidate for dissociation. A slightly more converted pathway is mediated by hydroperoxide_4 and is accompanied by intramolecular H atom transfer, analogous to the dissociation pathway found for CysH$^+$ + $^1O_2$. During three-body dissociation of hydroperoxide_4, the H atom of the hydroperoxyl group which originally belongs to NH$_3^+$ is transferred to C$^\alpha$ of the backbone, ejecting a neutral glycine molecule H$_2$NCH$_2$CO$_2$H and ground-state O$_2$. Because of the high stability of glycine, this dissociation pathway becomes more energetically favorable than the dioxetane- or hydroperoxide_3-mediated one, and is actually slightly exothermic (-0.04 eV).

IV. CONCLUSIONS

The present study employs guided-ion-beam tandem mass spectrometry to determine the reaction products, cross sections, and collision energy dependence for the reactions of CysH$^+$ and TrpH$^+$ with electronically excited singlet molecular oxygen (a $^1\Delta_g$). DFT calculations were carried out to identify the reaction coordinates (including reactants, intermediate complexes, transition states, and products), and investigate thermodynamics and energy barriers. Quasi-classical, direct dynamics trajectory simulations were performed for collisions of CysH$^+$ with $^1O_2$ at collision energies of 0.2 and 0.3 eV. Trajectories demonstrate the importance of a complex-mediated mechanism at low E_{col}, and reveal a number of interesting dynamics features including orientation dependence for reaction. One of the most interesting results is that the electronic excitation energy of $^1O_2$ can be used to drive the dissociation of CysH$^+$ and TrpH$^+$. The dissociative excitation energy transfer has to be mediated by intermediate complexes, and only becomes important at low E_{col} when the complexes have significant lifetimes. Within these complexes, there exists charge delocalization or intramolecular charge transfer. This could induce strong electronic interaction between CysH$^+$/TrpH$^+$ and $^1O_2$, and that probably explains the transitions to triplet dissociation channels. This work exemplifies another system of dissociative excitation transfer of $^1O_2$, in addition to the dissociation of OH$^-$(H$_2$O)$_{1,2}$ by $^1O_2$ reported by Viggiano et al.[48]

■ AUTHOR INFORMATION

Corresponding Author
*E-mail: jianbo.liu@qc.cuny.edu.

■ REFERENCES

(1) Schweitzer, C.; Schmidt, R. *Chem. Rev.* **2003**, *103*, 1685.
(2) Frimer, A. A. *Singlet O₂, Vol I, Physical-Chemical Aspects*; CRC Press: Boca Raton, FL, 1985.
(3) Frimer, A. A. *Singlet O₂, Vol II, Reaction Modes and Products, Part 1*; CRC Press: Boca Raton, FL, 1985.
(4) Frimer, A. A. *Singlet O₂, Vol III, Reaction Modes and Products, Part 2*; CRC Press: Boca Raton, FL, 1985.
(5) Frimer, A. A. *Singlet O₂, Vol IV, Polymers and Biomolecules*; CRC Press: Boca Raton, FL, 1985.
(6) Sawyer, D. T. *Oxygen Chemistry*; Oxford University Press: New York, 1991.
(7) Ogilby, P. R. *Chem. Soc. Rev.* **2010**, *39*, 3181.
(8) Davies, M. J. *Biochem. Biophys. Res. Commun.* **2003**, *305*, 761.
(9) Morgan, P. E.; Dean, R. T.; Davies, M. J. *Free Radical Biol. Med.* **2004**, *36*, 484.
(10) Davies, M. J. *Biochim. Biophys. Acta* **2005**, *1703*, 93.
(11) Palumbo, G. *Expert Opin. Drug Delivery* **2007**, *4*, 131.
(12) Davies, M. J. *Photochem. Photobiol. Sci.* **2004**, *3*, 17.
(13) Hedin, E. M. K.; Patkar, S. A.; Vind, J.; Svendsen, A.; Hult, K.; Berglund, P. *Can. J. Chem.* **2002**, *80*, 529.
(14) Gracanin, M.; Hawkins, C. L.; Pattison, D. I.; Davies, M. J. *Free Radical Biol. Med.* **2009**, *47*, 92.
(15) Anastasio, C.; McGregor, K. G. *Atmos. Environ.* **2001**, *35*, 1079.
(16) McGregor, K. G.; Anastasio, C. *Atmos. Environ.* **2001**, *35*, 1091.
(17) Mader, B. T.; Yu, J. Z.; Xu, J. H.; Li, Q. F.; Hu, W. S.; Flagan, R. C.; Seinfeld, J. H. *J. Geophys. Res.* **2004**, *109*, D06206.
(18) Anastasio, C.; McGregor, K. G. *Aerosol Sci. Technol.* **2000**, *32*, 106.
(19) Matsumoto, K.; Uematsu, M. *Atmos. Environ.* **2005**, *39*, 2163.
(20) Fishman, P. H.; Kusiak, J. W.; Bailey, J. M. *Biochem.* **1973**, *12*, 2540.
(21) Gennari, G.; Gauzzo, G.; Jori, G. *Photochem. Photobiol.* **1974**, *20*, 497.
(22) Cannistraro, S.; Jori, G.; Vorst, A. V. d. *Photochem. Photobiol.* **1978**, *27*, 517.
(23) Straight, R. C.; Spikes, J. D. Photosensitized oxidation of biomolecules. In *Singlet O₂*; Frimer, A. A., Ed.; CRC Press: Boca Raton, FL, 1985; Vol. 4: Polymers and Biomolecules; p 91.
(24) Ando, W.; Takata, T. Photooxidation of sulfur compounds. In *Singlet O₂*; Frimer, A. A., Ed.; CRC Press: Boca Raton, 1985; Vol. 3: Reaction Modes and Products Part 2; p 1.
(25) Rougee, M.; Bensasson, R. V.; Land, E. J.; Pariente, R. *Photochem. Photobiol.* **1988**, *47*, 485.
(26) Justo, G. Z.; Camargo, F. A.; Haun, M.; Faljoni-Alario, A.; Duran, N. *Physiol. Chem. Phys. Med. NMR* **2000**, *32*, 145.
(27) Nakagawa, M.; Yoshikawa, K.; Hino, T. *J. Am. Chem. Soc.* **1975**, *97*, 6496.
(28) Nakagawa, M.; Okajima, H.; Hino, T. *J. Am. Chem. Soc.* **1977**, *99*, 4424.
(29) Nakagawa, M.; Watanabe, H.; Kodato, S.; Okajima, H.; Hino, T.; Flippen, J. L.; Witkop, B. *Proc. Natl. Acad. Sci. U.S.A.* **1977**, *74*, 4730.

(30) Saito, I.; Matsuura, T.; Nakagawa, M.; Hino, T. *Acc. Chem. Res.* **1977**, *10*, 346.

(31) Langlots, R.; H. Ali, N. B.; Wagner, J. R.; Lier, J. E. v. *Photochem. Photobiol.* **1986**, *44*, 117.

(32) Grosvenor, A. J.; Morton, J. D.; Dyer, J. M. *Amino Acids* **2010**, *39*, 285.

(33) Fang, Y.; Liu, J. *J. Phys. Chem. A* **2009**, *113*, 11250.

(34) Fang, Y.; Liu, F.; Bennett, A.; Ara, S.; Liu, J. *J. Phys. Chem. B* **2011**, *115*, 2671.

(35) Yamashita, M.; Fenn, J. B. *J. Phys. Chem.* **1984**, *88*, 4451.

(36) Fenn, J. B.; Mann, M.; Meng, C. K.; Wong, S. F.; Whitehouse, C. M. *Science* **1989**, *246*, 64.

(37) Gerlich, D. Inhomogeneous RF fields: A versatile tool for the study of processes with slow ions. In *State-Selected and State-to-State Ion—Molecule Reaction Dynamics. Part I. Experiment*; Ng, C. Y., Baer, M., Eds.; John Wiley & Sons, Inc.: New York, 1992; Vol. 82; p 1.

(38) Fehsenfeld, F. C.; Albritton, D. L.; Burt, J. A.; Schiff, H. I. *Can. J. Chem.* **1969**, *47*, 1793.

(39) Schmitt, R. J.; Bierbaum, V. M.; DePuy, C. H. *J. Am. Chem. Soc.* **1979**, *101*, 6443.

(40) Bierbaum, V. M.; Schmitt, R. J.; DePuy, C. H. *Environ. Heath Perspect.* **1980**, *36*, 119.

(41) Grabowski, J. J.; Van Doren, J. M.; DePuy, C. H.; Bierbaum, V. M. *J. Chem. phys.* **1984**, *80*, 575.

(42) Dotan, I.; Barlow, S. E.; Ferguson, E. E. *Chem. Phys. Lett.* **1985**, *121*, 38.

(43) Upschulte, B. L.; Marinelli, W. J.; Green, B. D. *J. Phys. Chem.* **1994**, *98*, 837.

(44) Midey, A.; Dotan, I.; Lee, S.; Rawlins, W. T.; Johnson, M. A.; Viggiano, A. A. *J. Phys. Chem. A* **2007**, *11*, 5218.

(45) Midey, A.; Dotan, I.; Viggiano, A. A. *J. Phys. Chem. A* **2008**, *112*, 3040.

(46) Midey, A. J.; Dotan, I.; Viggiano, A. A. *Int. J. Mass Spectrom.* **2008**, *273*, 7.

(47) Midey, A.; Dotan, I.; Seeley, J. V.; Viggiano, A. A. *Int. J. Mass Spectrom.* **2009**, *280*, 6.

(48) Viggiano, A. A.; Midey, A.; Eyet, N.; Bierbaum, V. M.; Troe, J. *J. Chem. Phys.* **2009**, *131*, 094303/1.

(49) Eyet, N.; Midey, A.; Bierbaum, V. M.; Viggiano, A. A. *J. Phys. Chem. A* **2010**, *114*, 1270.

(50) Eyet, N.; Viggiano, A. A. *J. Phys. Chem. A* **2010**, *114*, 7506.

(51) Fang, Y.; Bennett, A.; Liu, J. *Int. J. Mass Spectrom.* **2010**, *293*, 12.

(52) Fang, Y.; Bennett, A.; Liu, J. *Phys. Chem. Chem. Phys.* **2011**, *13*, 1466.

(53) Moision, R. M.; Armentrout, P. B. *J. Am. Soc. Mass Spectrom.* **2007**, *18*, 1124.

(54) Krutchinsky, A. N.; Chernushevich, I. V.; Spicer, V. L.; Ens, W.; Standing, K. G. *J. Am. Soc. Mass Spectrom.* **1998**, *9*, 569.

(55) Douglas, D. J.; French, J. B. *J. Am. Mass Spectrom.* **1992**, *3*, 398.

(56) Ervin, K. M.; Armentrout, P. B. *J. Chem. Phys.* **1985**, *83*, 166.

(57) Armentrout, P. B. *J. Anal. At. Spectrom.* **2004**, *19*, 571.

(58) Seliger, H. H. *Anal. Biochem.* **1960**, *1*, 60.

(59) Khan, A.; Kasha, M. *J. Chem. Phys.* **1963**, *39*, 2105.

(60) McDermott, W. E.; Pchelkin, N. R.; Benard, D. J.; Bousek, R. R. *Appl. Phys. Lett.* **1978**, *32*, 469.

(61) Lafferty, W. J.; Solodov, A. M.; Lugez, C. L.; Fraser, G. T. *Appl. Opt.* **1998**, *37*, 2264.

(62) Troe, J. *Chem. Phys. Lett.* **1985**, *122*, 425.

(63) Frisch, M. J.; Trucks, G. W.; Schlegel, H. B.; Scuseria, G. E.; Robb, M. A.; Cheeseman, J. R.; Scalmani, G.; Barone, V.; Mennucci, B.; Petersson, G. A.; Nakatsuji, H.; Caricato, M.; Li, X.; Hratchian, H. P.; Izmaylov, A. F.; Bloino, J.; Zheng, G.; Sonnenberg, J. L.; Hada, M.; Ehara, M.; Toyota, K.; Fukuda, R.; Hasegawa, J.; Ishida, M.; Nakajima, T.; Honda, Y.; Kitao, O.; Nakai, H.; Vreven, T.; Montgomery, J. A., Jr.; Peralta, J. E.; Ogliaro, F.; Bearpark, M.; Heyd, J. J.; Brothers, E.; Kudin, K. N.; Staroverov, V. N.; Keith, T.; Kobayashi, R.; Normand, J.; Raghavachari, K.; Rendell, A.; Burant, J. C.; Iyengar, S. S.; Tomasi, J.; Cossi, M.; Rega, N.; Millam, J. M.; Klene, M.; Knox, J. E.; Cross, J. B.; Bakken, V.; Adamo, C.; Jaramillo, J.; Gomperts, R.; Stratmann, R. E.; Yazyev, O.; Austin, A. J.; Cammi, R.; Pomelli, C.; Ochterski, J. W.; Martin, R. L.; Morokuma, K.; Zakrzewski, V. G.; Voth, G. A.; Salvador, P.; Dannenberg, J. J.; Dapprich, S.; Daniels, A. D.; Farkas, O.; Foresman, J. B.; Ortiz, J. V.; Cioslowski, J.; Fox, D. J. *Gaussian 09, Revision B. 01*; Gaussian, Inc.: Wallingford CT, 2009.

(64) Matxain, J. M.; Ristilae, M.; Strid, A.; Eriksson, L. A. *Chem.—Eur. J.* **2007**, *13*, 4636.

(65) Zheng, J.; Alecu, I. M.; Lynch, B. J.; Zhao, Y.; Truhlar, D. G. Database of Frequency Scale Factors for Electronic Model Chemistries, Version 2; available at http://comp.chem.umn.edu/freqscale/version2.htm, 2010.

(66) Hase, W. L.; Bolton, K.; de Sainte Claire, P.; Duchovic, R. J.; Hu, X.; Komornicki, A.; Li, G.; Lim, K.; Lu, D.; Peslherbe, G. H.; Song, K.; Swamy, K. N.; Vande Linde, S. R.; Varandas, A.; Wang, H.; Wolf, R. J. *VENUS99: A general chemical dynamics computer program*; Texas Tech Univeristy: Lubbock, TX, 1999.

(67) Bakken, V.; Millam, J. M.; Schlegel, H. B. *J. Chem. Phys.* **1999**, *111*, 8773.

(68) Bacskay, G. B. *Chem. Phys.* **1981**, *61*, 385.

(69) Laaksonen, L. gOpenMol; 3.0 ed.; Center for Scientific Computing: Espoo, Finland, 2005; available at www.csc.fi/gopenmol/.

(70) Liu, J.; Song, K.; Hase, W. L.; Anderson, S. L. *J. Chem. Phys.* **2003**, *119*, 3040.

(71) Liu, J.; Song, K.; Hase, W. L.; Anderson, S. L. *J. Phys. Chem. A* **2005**, *109*, 11376.

(72) Liu, J.; Uselman, B.; Boyle, J.; Anderson, S. L. *J. Chem. Phys.* **2006**, *125*, 133115.

(73) Kulik, W.; Heerma, W. *Biomed. Environ. Mass Spectrom.* **1988**, *15*, 419.

(74) Dookeran, N. N.; Yalcin, T.; Harrison, A. G. *J Mass Spectrom* **1996**, *31*, 500.

(75) Burrows, E. P. *J. Mass Spectrom.* **1998**, *33*, 221.

(76) O'Hair, R. A. J.; Stylesa, M. L.; Reid, G. E. *J. Am. Soc. Mass Spectrom.* **1998**, *9*, 1275.

(77) Rogalewicz, F.; Hoppilliard, Y.; Ohanessian, G. *Int. J. Mass Spectrom.* **2000**, *195/196*, 565.

(78) El Aribi, H.; Orlova, G.; Hopkinson, A. C.; Siu, K. W. M. *J. Phys. Chem. A* **2004**, *108*, 3844.

(79) Lioe, H.; O'Hair, R. A. J.; Reid, G. E. *J. Am. Soc. Mass Spectrom.* **2004**, *15*, 65.

(80) Lioe, H.; O'Hair, R. A. J. *Anal. Bioanal. Chem.* **2007**, *389* 1429.

(81) Liu, J.; Van Devener, B.; Anderson, S. L. *J. Chem. Phys.* **2002**, *116*, 5530.

(82) Hogg, P. J. *Trends Biochem. Sci.* **2004**, *28*, 210.

(83) Matheson, I. B. C.; He, J. *Photochem. Photobiol.* **1979**, *29*, 879.

(84) Palumbo, M. C.; Garcia, N. A.; Arguello, G. A. *J. Photochem. Photobiol. B: Biol* **1990**, *7*, 33.

(85) Leach, A. R. *Molecular modeling: Principles and applications*; Pearson, Prentice Hall: Harlow, England, 2001.

(86) Maksic, Z. B.; Kovacevic, B. *Chem. Phys. Lett.* **1999**, *307*, 497.

(87) Gao, B.; Wyttenbach, T.; Bower, M. T. *J. Am. Chem. Soc.* **2009**, *131*, 4695.

(88) Citir, M.; Stennett, E. M. S.; Oomens, J.; Steill, J. D.; Rodgers, M. T.; Armentrout, P. B. *Int. J. Mass Spectrom.* **2010**, *297*, 9.

(89) Mino, W. K.; Jr., K. G.; Wang, D.; Stedwell, C. N.; Polfer, N. C. *J. Phys. Chem. Lett.* **2011**, *2*, 299.

(90) Grégoire, G.; Jouvet, C.; Dedonder, C.; Sobolewski, A. L. *Chem. Phys.* **2006**, *324*, 398.

(91) Grégoire, G.; Jouvet, C.; Dedonder, C.; Sobolewski, A. L. *J. Am. Chem. Soc.* **2007**, *129*, 6223.

(92) Wilkinson, F.; Helman, W. P.; Ross, A. B. *J. Phys. Chem. Ref. Data* **1995**, *24*, 663.

(93) Liu, J.; Devener, B. V.; Anderson, S. L. *J. Chem. Phys.* **2002**, *117*, 8292.

(94) Kang, H.; Dedonder-Lardeux, C.; Jouvet, C.; Grégoire, G.; Desfrancois, C.; Schermann, J.-P.; Barat, M.; Fayeton, J. A. *J. Phys. Chem. A* **2005**, *109*, 2417.

9908

dx.doi.org/10.1021/jp205235d |*J. Phys. Chem. B* 2011, 115, 9898–9909

(95) Lepère, V.; B. Lucas, M. B.; Fayeton, J. A.; Picard, V. J.; Jouvet, C.; Çarçabal, P.; Nielsen, I.; Dedonder-Lardeux, C.; Grégoire, G.; Fujii, A. *J. Chem. Phys.* **2007**, *127*, 134313.

(96) Lucas, B.; Barat, M.; Fayeton, J. A.; Perot, M.; Jouvet, C.; Grégoire, G.; Nielsen, S. B. *J. Chem. Phys.* **2008**, *128*, 164302.

(97) Grégoire, G.; Lucas, B.; Barat, M.; Fayeton, J. A.; Dedonder-Lardeux, C.; Jouvet, C. *Eur. Phys. J. D* **2009**, *51*, 109.